Earth and Planetary Science Letters 404 (2014) 167–177

Contents lists available at ScienceDirect

Earth and Planetary Science Letters

www.elsevier.com/locate/epsl

High latitude hydrological changes during the Eocene Thermal Maximum 2

Srinath Krishnan [a,*], Mark Pagani [a,1], Matthew Huber [b], Appy Sluijs [c,2]

[a] Department of Geology and Geophysics, Yale University, New Haven, CT 06211, USA
[b] University of New Hampshire, Department of Earth Sciences, Durham, NH 03824, USA
[c] Department of Earth Sciences, Faculty of Geosciences, Utrecht University, Laboratory of Paleobotany and Palynology, Budapestlaan 4, 3583 CD Utrecht, The Netherlands

ARTICLE INFO

Article history:
Received 21 December 2013
Received in revised form 26 June 2014
Accepted 25 July 2014
Available online xxxx
Editor: G.M. Henderson

Keywords:
Eocene Thermal Maximum 2
Eocene hyperthermals
n-alkanes
leaf waxes
hydrogen isotopes
hydrological cycle

ABSTRACT

The Eocene hyperthermals, including the Paleocene–Eocene Thermal Maximum (PETM) and Eocene Thermal Maximum 2 (ETM2), represent extreme global warming events ~56 and 54 million years ago associated with rapid increases in atmospheric greenhouse gas concentrations. An initial study on PETM characteristics in the Arctic region argued for intensification of the hydrological cycle and a substantial increase in poleward moisture transport during global warming based on compound-specific carbon and hydrogen isotopic ($^2H/^1H$) records from sedimentary leaf-wax lipids. In this study, we apply this isotopic and hydrological approach on sediments deposited during ETM2 from the Lomonosov Ridge (Integrated Ocean Drilling Program Expedition 302). Our results show similar $^2H/^1H$ changes during ETM2 as during the PETM, with a period of ^2H-enrichment (~20‰) relative to "pre-event" values just prior to the negative carbon isotope shift (CIE) that is often taken as the onset of the hyperthermal, and more negative lipid δ^2H values (~ −15‰) during peak warming. Notably, lipid ^2H-enrichment at the base of the event is coeval with colder TEX_{86}^H temperatures.

If $^2H/^1H$ values of leaf waxes primarily reflect the hydrogen isotopic composition of precipitation, the observed local relationship between temperature and $^2H/^1H$ values for the body of ETM2 is precisely the opposite of what would be predicted using a simple Rayleigh isotope distillation model, assuming a meridional vapor trajectory and a reduction in equator-pole temperature gradients. Overall, a negative correlation exists between the average chain length of *n*-alkanes and $^2H/^1H$ suggesting that local changes in ecology could have impacted the hydrogen isotopic compositions of leaf waxes. The negative correlation falls across three separate intervals — the base of the event, the initial CIE, and during the H2 hyperthermal (of which the assignment is not fully certain). Three possible mechanisms potentially explain ^2H-enriched signals at the base of the event, including (1) intense local drying and cooling leading to evaporative ^2H-enrichment; (2) changes in frequency/intensity of storm events and its impact on high latitude amount effects; and (3) changes in low-latitude temperatures. Evidence for hydrological shifts at the base of both hyperthermals suggests that hydrological change or the factors promoting hydrological change played a role in triggering the release of greenhouse gases. Generation of similar high-resolution isotopic- and temperature records at other latitudes is crucial for understanding the causal links between temperature and hydrological changes and may help constrain the source and mechanism of carbon release that triggered the early Eocene hyperthermals.

© 2014 Elsevier B.V. All rights reserved.

1. Introduction

The impact of greenhouse-gas induced warming on the character of the global hydrological cycle has been a matter of widespread debate in the climate community (Allan and Soden, 2007; Allen and Ingram, 2002; Barron et al., 1989; Held and Soden, 2006; Huntington, 2006; Trenberth, 2011; Wentz et al., 2007). The general view is that warming intensifies the global hydrological cycle, but an intensified cycle does not simply imply a wetter world (Pierrehumbert, 2002). Rather, it refers to an increase in the intensity of evaporation in evaporative zones with a compensating increase in moisture delivery in regions that experience net precipitation. Held and Soden (2006), in their assessment of coupled

* Corresponding author. Tel.: +1 203 432 8343; fax: +1 203 432 3134.
E-mail addresses: srinath.krishnan@yale.edu (S. Krishnan), mark.pagani@yale.edu (M. Pagani), matthew.huber@unh.edu (M. Huber), A.sluijs@uu.nl (A. Sluijs).
[1] Tel.: +1 203 432 6275; fax: +1 203 432 3134.
[2] Tel.: +31 302532638.

http://dx.doi.org/10.1016/j.epsl.2014.07.029
0012-821X/© 2014 Elsevier B.V. All rights reserved.

climate simulations, find global enhancement of evaporation–precipitation (E-P) spatial patterns under future climate change scenarios. Outside of the tropics, they find that modern E-P zones are located in the mid to high latitudes and global warming is expected to result in midlatitude drying and increased poleward moisture transport. However, confidence in these projections is limited by the lack of long-term data required for validation. Modern day satellite measurements and documented historical observations (NRC, 2006) do not capture the magnitude of temperature changes predicted under future scenarios of CO_2 emission. As a consequence, ancient records of climate when global temperatures were substantially elevated above modern conditions need to be explored.

Several rapid and extreme transient global warming events, termed hyperthermals, occurred during the late Paleocene and early Eocene (Thomas and Zachos, 2000; Lourens et al., 2005; Cramer et al., 2003). Global average temperatures during hyperthermals rose by as much as 5 °C above pre-event temperatures (e.g., Dunkley Jones et al., 2013) that were already at least 10 °C warmer than today (Huber and Caballero, 2011; Lunt et al., 2012), and thus provide case studies of hydrological characteristics under a much warmer world. Hyperthermals are characterized by substantial carbonate dissolution associated with shoaling of the calcite compensation depth, and negative carbon isotopic excursions (CIE) (e.g., Bralower et al., 1997; Schmitz et al., 1996; Zachos et al., 2005; Stap et al., 2009) that implicate a massive and rapid increase in ocean–atmosphere CO_2 concentrations (Dickens et al., 1995, 1997; Lourens et al., 2005; Sluijs et al., 2009). Accordingly, these events are often referred to as extreme end-member scenarios of modern day greenhouse gas-induced global warming (Pagani et al., 2006; Zachos et al., 2004; Abels et al., 2012).

During the Paleocene–Eocene Thermal Maximum (PETM; ∼55 Ma), global average surface temperatures rose by 4–5 °C (Dunkley Jones et al., 2013), with some regional variations (Kennett and Stott, 1991; Thomas et al., 1999; Zachos et al., 2003, 2006; Wing et al., 2005; Sluijs et al., 2006, 2011). The magnitude of the negative CIE ranges from ∼ −2.5 to −6‰, in terrestrial and marine carbonates (e.g., Zachos et al., 2007; Bowen et al., 2004), paleosols (Koch et al., 1992), organic matter (Sluijs and Dickens, 2012), and biomarkers of higher-plants (Pagani et al., 2006; Schouten et al., 2007; Smith et al., 2007) and marine archaea (Schoon et al., 2013). ETM2 is more poorly studied, but records indicate several geochemical characteristics similar to the PETM, including a negative CIE approximately half the magnitude of PETM (Lourens et al., 2005; Sluijs et al., 2009; Stap et al., 2010; Schoon et al., 2011). Another warming event (termed H2) following ETM2 by approximately 100 kyrs, is also associated with deep ocean carbonate dissolution and a negative carbon isotope excursion (Cramer et al., 2003; Stap et al., 2010).

During ETM2, TEX_{86}-based sea surface temperatures, pollen data and dinoflagellate records from the Lomonosov Ridge, Arctic Ocean (∼85°N paleolatitude; Integrated Ocean Drilling Program Expedition 302; Arctic Coring Expedition; ACEX) suggest sea-surface temperatures (SST) increased ∼3–5 °C, with evidence for tropical vegetation on land and a decrease in sea surface salinity (Sluijs et al., 2009). Due to oceanographic changes and possible vertical water-column migration of archaea, the production depth of the lipids used in the TEX_{86} proxy, temperature estimates and peak warming are not well constrained (Sluijs et al., 2009). The current assessment argues that temperature and hydrographic responses to increased CO_2 during ETM2 in the Arctic region are similar to the changes observed for the PETM, but at a smaller scale.

A range of hypotheses have been proposed to explain the source of carbon driving early Eocene hyperthermals, including dissociation of methane hydrates (Dickens et al., 1995, 1997; Lunt et al., 2011), conflagration of peat deposits (Kurtz, 2003), intrusive-heating of organic-rich marine sediments (Svenson et al., 2004), drying of restricted seaways leading to oxidation of organic matter (Higgins and Schrag, 2006), bolide impact (Kent et al., 2003; Wright and Schaller, 2013), extreme tropical warmth resulting in death and oxidation of plant matter (Huber, 2009) and high latitude permafrost oxidation (DeConto et al., 2012). An early increase of global or regional temperatures prior to the release of $\delta^{13}C$-depleted carbon has been argued as the reason for initiation of the PETM (Sluijs et al., 2007; Eldrett et al., 2014), but at present, there is no evidence for warming leading the CIE during ETM2. Poor temporal resolution of temperature records with respect to carbon isotope records, as well as the accuracy of absolute temperature values, limits our capacity to constrain the timing of initial temperature shifts and to firmly establish lead–lag relationships (e.g., Sluijs et al., 2007). Improved linkages between carbon input, global temperature perturbations, runoff characteristics and the hydrological cycle, investigations of hydrological changes could provide an alternative path for assessing the character of climate change prior to- and during hyperthermals.

Hydrological perturbations during the PETM and other hyperthermals have been investigated using various methodologies. Leaf Margin Analysis and changes in macro-flora at the Cabin Fork section (Wyoming) shows an ∼40% decline in precipitation at the onset of the PETM followed by increased precipitation during the latter part of the event (Wing et al., 2005). Continental records in the Spanish Pyrenees across the Paleocene/Eocene boundary indicate a change from semiarid coastal plain deposits to conglomerate braid deposits (interpreted to be proximal parts of a mega-fan; Schmitz and Pujalte, 2007), suggesting increased seasonality, intensified intra-annual humidity gradients and more intense precipitation events. Bowen et al. (2004) used soil–carbon modeling to argue that the offset between the magnitude of the terrestrial and marine CIEs during the PETM in the northern midlatitudes could be explained by an increase in relative humidity (RH) and/or soil moisture. Many shelf sections show an increase in the supply of terrigenous material during several hyperthermals, suggesting more intense weathering (Hollis et al., 2005; Giusberti et al., 2007; Nicolo et al., 2007; Sluijs et al., 2008a; Slotnick et al., 2012; see overview in Sluijs et al., 2008b). Proliferations of fresh-water tolerant dinoflagellates and increases in the supply of terrestrial pollen and spores have been related to increased river runoff (Crouch et al., 2003; Sluijs et al., 2006; Sluijs and Brinkhuis, 2009; Harding et al., 2011). Finally, pollen assemblages have been used to assess hydrological changes and regionally found to lead the carbon isotope excursion across the onset of the PETM (Eldrett et al., 2014).

Hydrogen isotope compositions of higher-plant leaf wax lipids preserved in sedimentary deposits (Huang et al., 1995; Polissar et al., 2009; Wilkie et al., 2013) have been used to interpret hydrological conditions during periods of climate change (Pagani et al., 2006; Tierney et al., 2010; Feakins et al., 2012; Schefuß et al., 2011), changes in the rates of evaporation and precipitation (E-P) (Huang et al., 2000, 2002; Xie et al., 2000; Andersen et al., 2001), and source–water composition (Schouten et al., 2006). Leaf waxes during the PETM have been analyzed in a range of localities including the tropics (Jaramillo et al., 2010; Handley et al., 2008, 2012), midlatitudes (Big Horn Basin, North America: Smith et al., 2007 and Forada, Italy: Tipple et al., 2011), and the high latitude Arctic Ocean (Pagani et al., 2006). Low-latitude leaf-wax *n*-alkane records from Venezuela show an ∼ −40‰ δ^2H shift at the base of the CIE (Jaramillo et al., 2010) and interpreted as reflecting increased precipitation and forest diversification. *n*-Alkane δ^2H records from the Big Horn Basin (Wyoming, USA) show an initial positive shift (∼5‰) at the base of the CIE and more negative values (∼10‰) during the body of the event (Smith et al., 2007). The direction of changes at the Big Horn Basin is remarkably similar to the $^2H/^1H$

record of Arctic PETM (Pagani et al., 2006), where a positive ~55‰ δ^2H shift occurs at the base of the event. Pagani et al. (2006) hypothesized that ^{2}H-enrichment prior to the warmth of the PETM reflected an early shift in hydrology resulting from an invigorated hydrological cycle and a reduction in the number of rainout events across the midlatitudes, with increased poleward moisture transport. During the peak of the CIE, n-C_{27} and n-C_{29} δ^2H values are more negative by as much as 20‰ relative to pre-event values, followed by a near recovery to pre-event ^{2}H/^{1}H compositions. In summary, available data suggest that substantial shifts in the hydrological cycle occurred during the PETM.

In this study, we present records of compound-specific carbon and hydrogen isotopic compositions of leaf-wax biomarkers for hyperthermal ETM2 from the high Arctic. We compare our results with PETM records generated from the same ocean core (Pagani et al., 2006) in order to assess similarities/differences in temporal patterns and magnitudes of change.

2. Materials and methods

Sediments for this study were recovered from the Lomonosov Ridge, a 1650 km fragment of continental crust that extends from Greenland to the Siberian Margin, during the Integrated Ocean Drilling Program (IODP) Expedition 302, the Arctic Coring Expedition (ACEX) (Fig. 1 in Backman et al., 2006). Average late Paleocene and early Eocene sedimentation rates at this site approximate 1 cm kyr^{-1} with the exception of significantly increased sedimentation (~5 cm kyr^{-1}) during the PETM (Sluijs et al., 2008a). ETM2 was identified based on dinocyst biostratigraphy (Sluijs et al., 2008a), a negative CIE in total organic carbon (Stein et al., 2006; Sluijs et al., 2009) and biomarkers of marine unicellular organisms (Schoon et al., 2011, 2013). We used splits of 25 samples that were also used in earlier work (Sluijs et al., 2009; Schoon et al., 2011, 2013) between the depths of 362 and 370 mcd that cover ETM2. Sediments are mostly laminated siliciclastic mudstones, with palynological and geochemical data indicating a nearshore environment and water-depths of ~200 m (Sluijs et al., 2008a; O'Regan et al., 2008). Sediments yield ample organic matter related to high productivity and good preservation resulting from low oxygen concentrations in the water column and at the sediment–water interface (e.g., Stein et al., 2006; Knies et al., 2008; Sluijs et al., 2008a, 2009; Schoon et al., 2011). Sluijs et al. (2009) also suggested the presence of H2 in the ACEX sediments based on the recognition of a CIE in total organic carbon. However, this assignment was later questioned based on compound-specific work (Schoon et al., 2011) but not fully rejected (Sluijs and Dickens, 2012).

Samples were freeze-dried for ~24 h and lightly rinsed with 100% dichloromethane to eliminate surface contamination from prior handling. ~50 g of powdered sediment was extracted using an Accelerated Solvent Extractor (ASE 300, Dionex) with 100% dichloromethane at 100 °C and 1200 psi. Total lipid extracts were separated into three sub-fractions via silica gel column chromatography using ~4 ml of 100% hexane, 100% dichloromethane, and 100% methanol. Cyclic and branched alkanes collected in the hexane fraction were separated from normal and isoalkanes by two rounds of urea adduction (Wakeham and Pease, 1992). The resulting n-alkane fraction was then passed through a column of silver nitrate to remove co-eluting unsaturated hydrocarbons.

2.1. Compound distributions

Relative abundances and distributions of n-alkanes were determined using a Thermo Trace 2000 Gas Chromatograph (GC) fitted with a programmable-temperature vaporization injector, flame ionization detector (FID), and a silica DB-1 phase column (60 m × 0.25 mm I.D, 0.25 μm film thickness) with helium as the carrier gas (flow rate: 2 ml/min). Initial GC temperature was held at 60 °C during sample injection for 2 min, increased at 15 °C/min to 320 °C and held at 320 °C for 30 min.

The n-alkane chain lengths were identified by comparison with elution times of known standards. Distributions were estimated using the average chain length (ACL):

$$ACL = \frac{(A_{25} \times 25) + (A_{27} \times 27) + (A_{29} \times 29) + (A_{31} \times 31)}{(A_{25} + A_{27} + A_{29} + A_{31})} \quad (1)$$

where A_n refers to the area under the peak of carbon-chain length n.

2.2. Isotopic compositions

Stable isotopic compositions were determined using a Thermo Trace 2000 GC coupled to a Finnigan MAT 253 mass spectrometer, interfaced with a GC-C III combustion system (for δ^{13}C analysis) or a High Temperature Conversion system (for δ^2H analysis). GC column, carrier flow, and the temperature program were identical to those used to determine compound distributions.

Isotopic values are calculated using

$$\delta = \left(\frac{R_{sample}}{R_{standard}} - 1 \right) \quad (2)$$

where R represents the δ^{13}C/^{12}C or ^{2}H/^{1}H abundance ratio for the sample and standard. δ^{13}C and δ^2H are isotopic ratios relative to VPDB and VSMOW based on an in-house reference gas calibrated against Oztech standard gases.

The H_3^+ factor, with a mean value of 15.7 p.p.m./nA ± 0.4 p.p.m./nA (1σ), was determined daily and corrected prior to δ^2H analysis. External standards (Mix A; Indiana University Biogeochemical Laboratories) used to normalize sample isotopic ratios were measured at different concentrations (standards range between 100–600 ng/uL, while sample range between 300–500 ng/uL) before sample analysis daily and after every four runs. Precision (1σ) for external standards was ±0.6‰ for δ^{13}C and ±6‰ for δ^2H. All samples are run in duplicate and the mean of the duplicate analyses are reported.

3. Results

3.1. Compound distributions

The saturated hydrocarbon fraction is dominated by long-chain n-alkanes between n-C_{25} and n-C_{31} and consistently shows an odd-over-even carbon number predominance representative of higher plant leaf waxes. Organic analyses of core material indicate that samples are thermally immature (Boucsein and Stein, 2009). The average chain length observed in the section pre- and post-ETM2 is ~28.6 ACL units. This increases to ~29 ACL units during the CIE (Fig. 1).

3.2. Carbon isotopic composition

All n-alkanes show similar patterns of δ^{13}C change (Fig. 1) across ETM2. The average pre-event δ^{13}C values for n-C_{25}, n-C_{27}, n-C_{29} and n-C_{31} are −30.5‰, −30.8‰, −30.5‰, and −30.25‰, respectively. The characteristic negative CIE that marks the ETM2 is observed at 368.9 mcd for n-C_{27}, n-C_{29} and n-C_{31}. The most negative δ^{13}C values reach −32.6‰ for n-C_{27}, and −32‰ for n-C_{25}, n-C_{29}, and n-C_{31}. The average magnitude of the CIEs in n-alkanes observed at the Lomonosov Ridge across ETM2 is ~ −1.6‰ compared to ~ −4.5 to −6‰ for the PETM. A second negative shift in δ^{13}C values is observed for all chain lengths between 368.5 and

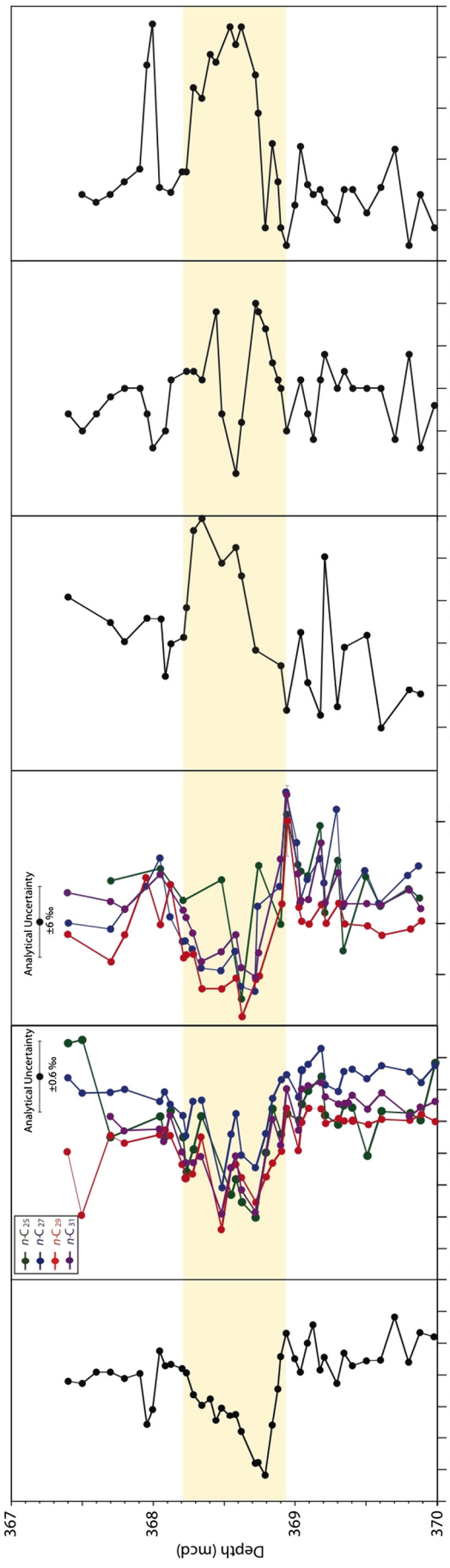

Fig. 1. Changes in $\delta^{13}C$ of total organic carbon (TOC; Sluijs et al., 2009), *n*-alkane $\delta^{13}C$, *n*-alkane $\delta^{2}H$, Average Chain Length (ACL), TEX'_{86} (Sluijs et al., 2009), and percentage low-salinity tolerant dinocysts (Sluijs et al., 2009) during Eocene Thermal Maximum 2 (ETM2). Shaded region indicates carbon isotopic excursion (CIE) associated with the hyperthermal. Analytical uncertainties for $\delta^{13}C$ and $\delta^{2}H$ values are based on precision of repeated analyses for an external standard (Mix A).

368.6 mcd. A recovery to near pre-CIE values occurs at the end of the ETM2 event. Due to low abundance of *n*-alkanes, we were unable to measure carbon isotopic compositions for the presumed H2 interval (between 367.8–368 mcd).

3.3. Hydrogen isotopic composition

All four homologs of higher-plant derived *n*-alkanes show broadly similar $^{2}H/^{1}H$ trends (Fig. 1). $^{2}H/^{1}H$ values prior to the event are −225‰ (*n*-C_{25}), −220‰ (*n*-C_{27}), −230‰ (*n*-C_{29}) and −225‰ (*n*-C_{31}). At the base of ETM2, $^{2}H/^{1}H$ values become ^{2}H-enriched by ∼15–20‰ for all chain lengths. The most positive $\delta^{2}H$ value observed is −204‰ for *n*-C_{31} and represents a maximum positive isotope shift of 21‰. During the CIE, $^{2}H/^{1}H$ values for all chain lengths become ^{2}H-depleted by ∼10–15‰ (relative to the early Eocene). A full recovery to pre-event $\delta^{2}H$ values occurs for all chain lengths. No substantial change in hydrogen isotopic composition is observed during the presumed H2 interval (between 367.8–368 mcd).

4. Discussion

4.1. Carbon isotopes

The magnitude of observed CIE during the ETM2 varies from ∼1.4‰ (in benthic foraminifera at Walvis Ridge; Stap et al., 2010) to ∼3.8‰ (in palaeosol carbonate nodules from the Bighorn Basin, Wyoming, USA; Abels et al., 2012). Sluijs et al. (2009) measured a CIE of ∼3.5‰ in total organic carbon at the Lomonosov Ridge, but it is clear that this value is affected by factors such as local carbon sources (for example, relative contributions of terrestrial versus marine organic matter), the isotopic composition of the local carbon pool, and changes in fractionation with increased pCO_2 concentrations (for a detailed discussion, see Sluijs and Dickens, 2012). To correct for input of terrestrial organic matter, Sluijs and Dickens (2012) used the Branched and Isoprenoid Tetraether (BIT) index proxy and estimated the CIE in marine organic matter to be ∼2.6‰. Marine biomarker-specific $\delta^{13}C$ presented by Schoon et al. (2011), show a CIE range of 3‰ to 4.5‰. They argued that this discrepancy is a result of increased isotope fractionation due to higher pCO_2 concentrations.

In our record, the drop in $\delta^{13}C_{n\text{-alkane}}$ values at the onset of ETM2 is synchronous with the $\delta^{13}C_{bulk}$ record (Fig. 1; Sluijs et al., 2009). While a smooth recovery to pre-event values is observed in $\delta^{13}C_{TOC}$, $\delta^{13}C_{n\text{-alkanes}}$ have a more complex recovery pattern. This pattern, with a second drop in $\delta^{13}C_{n\text{-alkanes}}$ at ∼368.48 mcd, is similar to trends observed in marine biomarkers, specifically phytanes and C_{25} HBI (Schoon et al., 2011). The magnitude of the $\delta^{13}C_{n\text{-alkane}}$ CIE during ETM2 is ∼ −1.6‰, within the observed range of existing ETM2 records (Cramer et al., 2003; Lourens et al., 2005; Galeotti et al., 2010; Stap et al., 2010; Schoon et al., 2011; Abels et al., 2012) and less than half the magnitude of CIE observed during the PETM from the same region (CIE of ∼ −4.5 to −6‰; Pagani et al., 2006).

It has been suggested that the Arctic PETM CIE is potentially biased by changes in vegetation and relative contributions of angiosperms and gymnosperms (Schouten et al., 2007; Sluijs and Dickens, 2012). Angiosperm-specific biomarker $\delta^{13}C$ values were found to be ∼3‰ more negative than aromatic compounds derived from gymnosperms (Schouten et al., 2007) during the PETM. This isotopic difference, as well a substantial increase in the relative amount of angiosperm over gymnosperm pollen was used to argue that the $\delta^{13}C_{n\text{-alkane}}$ record overestimates the magnitude of the CIE. Indeed, on average, modern angiosperms $\delta^{13}C$ values are about ∼2‰ more negative relative to gymnosperms (Pedentchouk et al., 2006; Diefendorf et al., 2011). Recent studies have used

pollen records in conjunction with biomarker analyses to constrain these impacts (Feakins et al., 2012; Feakins, 2013), but these evaluations are not straightforward, as pollen and *n*-alkanes can have different transport pathways to marine/terrestrial sediments (Conte and Webber, 2002; Schouten et al., 2007). Also, this interpretation is complicated by differences in the amount of *n*-alkane production between various vegetation types. Angiosperms, on average, produce up to 200 times more *n*-alkanes relative to co-existing gymnosperms today (Diefendorf et al., 2011; Bush and McInerney, 2013). Therefore, in the presence of angiosperms, the corresponding soil and sedimentary *n*-alkane records are likely biased to angiosperm values. Indeed, when differences in plant-functional types were considered in relationship to *n*-alkane $\delta^{13}C$ records, a 5.6‰ negative isotope excursion was estimated for the PETM (Diefendorf et al., 2011), similar to CIE of −6‰ and −4.5‰ determined from *n*-C_{27} and *n*-C_{29} *n*-alkanes respectively, in the Arctic (Pagani et al., 2006).

In this study, a simple explanation for the muted nature of the CIE observed in this record is that peak-CIE values are not captured in this record. However, this explanation is not supported by comparisons with the $\delta^{13}C_{TOC}$ record (Fig. 1) and marine biomarkers (Fig. 3b in Schoon et al., 2011). Alternatively, the similarity between the magnitude of the CIE observed in our $\delta^{13}C_{n\text{-alkane}}$ record and single-specimen biomarker records from Walvis Ridge (Stap et al., 2010) potentially indicates that the $\delta^{13}C_{n\text{-alkane}}$ records reflect the true magnitude of atmospheric CIE during the ETM2.

4.2. Hydrogen isotopes

Higher-plant hydrogen isotopic signatures are primarily set by the isotopic composition of the meteoric water and modified by physiological and environmental factors (see review in Sachse et al., 2012). Differences in the hydrogen isotope values of higher-plant *n*-alkanes have been observed in modern plants (Hou et al., 2007; Pedentchouk et al., 2008; Polissar and Freeman, 2010). These differences have been linked to several factors, including source–water compositions, biosynthetic pathways and soil/leaf evapotranspiration (Polissar and Freeman, 2010; Sachse et al., 2012). Water is transported through the stem to the leaves where fatty acids and *n*-alkanes are synthesized (Feakins and Sessions, 2010). Evapotranspiration can substantially alter $\delta^{2}H_{leaf}$ (Smith and Freeman, 2006). Evapotranspiration is closely related to "above-leaf" humidity that drives the water gradient between the leaf and the atmosphere. Based on a compilation of existing *n*-alkane $\delta^{2}H$ studies, Sachse et al. (2012) noted linear relations between $^{2}H/^{1}H$ values and relative humidity (for RH<70%) and evapotranspiration rates (for evapotranspiration rates up to 1000 mm yr^{-1}). Further, substantial isotopic differences have been found between vegetation at lower and higher latitudes. A large variance in $\delta^{2}H_{wax}$ (up to 60‰) was observed along a latitudinal transect across southeastern Mexico and northern Central America, even though $\delta^{2}H_{water}$ varied by only 25‰ (Douglas et al., 2012). It was suggested that this variance is primarily controlled by differences in aridity, with a secondary influence of vegetation-type on $\delta^{2}H_{n\text{-acids}}$ (Douglas et al., 2012). Greenhouse experiments show that the apparent hydrogen isotope fractionation factor for high-latitude light conditions is ~30–80‰ larger than those cited for the midlatitudes, indicating a potential effect of increased transpiration during the long Arctic summer day (Yang et al., 2011).

Given the known factors controlling modern plant $^{2}H/^{1}H$ compositions, shifts in Eocene Arctic $\delta^{2}H_{n\text{-alkane}}$ values could have resulted from changes in vegetation/plant communities, runoff or *n*-alkane sources, local evaporation, and global moisture transport. Ecosystem changes can influence the expression of biomarker $^{2}H/^{1}H$ records and changes in Arctic vegetation during the PETM have been inferred through both biomarker and pollen records (Sluijs et al., 2006; Schouten et al., 2007). During the PETM, gymnosperm-dominated ecosystems were largely replaced by angiosperm-dominated forests as temperatures increased (Sluijs et al., 2006; Schouten et al., 2007).

Approaches used to evaluate changes in ecosystem and plant community structure utilize pollen records (Feakins et al., 2012) or analyze changes in *n*-alkane distributions and average *n*-alkane carbon chain lengths. Palynological evaluations for ETM2 at Lomonosov Ridge indicate the overwhelming presence of conifer pollen such as Metasequioa-type (Taxodiaceae) and Pinus (pine) leading up to the event, and the appearance of palm pollen (Areciptes microreticulates) during ETM2 (Sluijs et al., 2009). In terms of ACL values, a recent study showed substantial inter- and intra-species variability and cautioned against its use for paleoecological reconstructions (Bush and McInerney, 2013). However, other studies have shown that ACL values are strongly related to environmental conditions including temperature, relative humidity, and vapor pressure deficit (Tipple and Pagani, 2012). For example, Tipple and Pagani (2012) demonstrated a linear relation between ACL and mean-annual temperatures across a latitudinal transect of the eastern United States, and Sachse et al. (2006) found a negative relation between the apparent hydrogen isotope fractionation and ACL. While the mechanistic reason for this relation remains unresolved, it is important to note that if ACL changes are a result of processes within a plant/leaf-surface during leaf-wax biosynthesis, then it is possible that these processes also impact $\delta^{2}H_{n\text{-alkane}}$ values. This change should be accounted for as a change in the apparent isotope enrichment factor and not $\delta^{2}H_{meteoric\text{-}water}$.

A short-lived, ~20‰ positive $\delta^{2}H_{n\text{-alkane}}$ shift at the base of the ETM2 is followed by a negative 15‰ shift within the CIE. A significant correlation exists between ACL and $^{2}H/^{1}H$ values during ETM2 (Fig. 2a). This relationship can be used to model $\delta^{2}H_{n\text{-alkane}}$ shifts if local changes in climate/environmental conditions that affect $\delta^{2}H_{wax}$ (i.e., unrelated to changes in the global hydrological cycle/moisture transport) were the primary determinant for plant $^{2}H/^{1}H$ (Fig. 2b). For this study, we restrict our discussion to three distinct time intervals (labeled DEV1, DEV2, and DEV3; Fig. 2b) where deviations from the ACL-$\delta^{2}H$ relationship are observed just prior to, during and following the CIE.

DEV1 represents a period of ^{2}H-enrichment prior to the CIE (368.5–368.9 m) with an insignificant change in *n*-alkane distributions suggesting limited changes in ecology and/or plant distributions. In modern non-arid environments, there is no overwhelming evidence for significant differences in $\delta^{2}H$ values between angiosperm and gymnosperm leaf waxes (Bi et al., 2005; Chikaraishi and Naraoka, 2003). Further, given that angiosperms produce up to 200 times more *n*-alkanes than co-existing gymnosperms (Diefendorf et al., 2011), changes in relative contributions of plant communities are not responsible for the expression of $\delta^{2}H$ values prior to the CIE. Alternatively; $^{2}H/^{1}H$ changes during DEV1 could have resulted from changes in biomarker provenance. Transport of terrestrially derived organic material occurs either through river discharge or eolian processes (de Leeuw et al., 1995; Hopmans et al., 2004; Pancost and Boot, 2004) and shifts in the location of fluvial discharge could potentially carry distinct biomarker signatures. However, it is generally assumed that fluvial discharge dominates over eolian transport, particularly in the Arctic during the Eocene (Sluijs et al., 2008a; Boucsein and Stein, 2009). During the early Cenozoic, the Arctic basin was an enclosed land-locked basin with limited connections to other oceans (Sluijs et al., 2009). Mineral grain size, high abundance of unique land-derived biomarkers, organic macerals and the low maturity of terrestrial macrofossils indicate close proximity of the Lomonosov Ridge to the coast (O'Reagan et al., 2008; Bouchsein and Stein, 2009). Kerogen maceral and organic carbon analyses in the ACEX core show substantial terrestrial input primarily derived from river

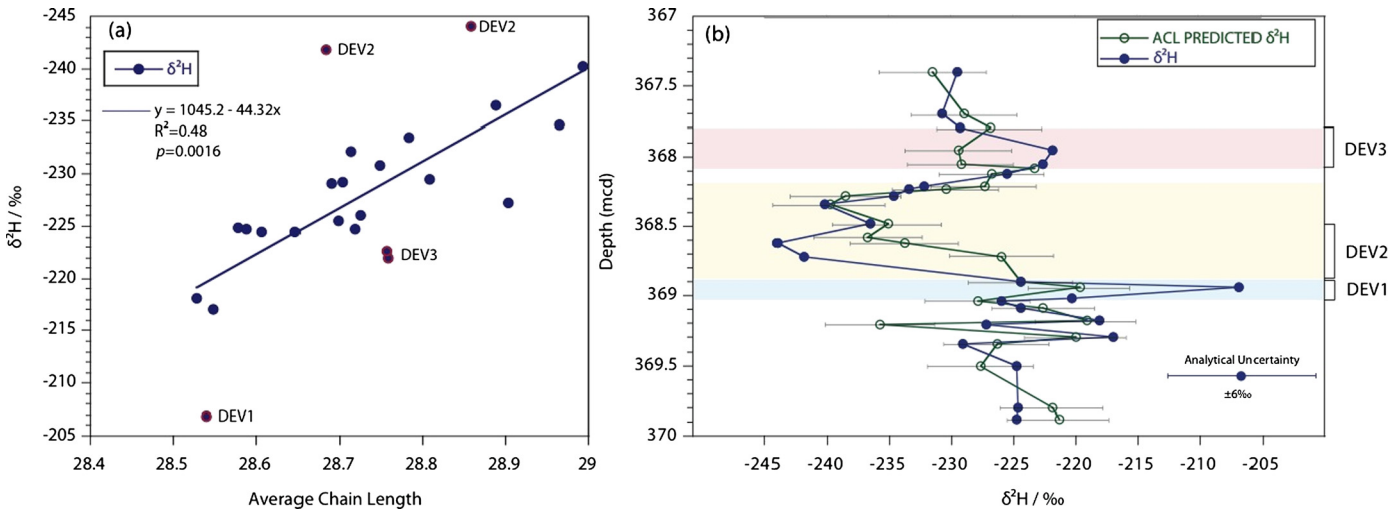

Fig. 2. (a) Relationship between average chain length (ACL) and mean-weighted average δ^2H and (b) changes in ACL predicted-*n*-alkane δ^2H during Eocene Thermal Maximum 2 (ETM2). ACL predicted δ^2H values are obtained by applying relationship in (a) to ACL values from Fig. 1. Red shaded region (DEV3) indicates carbon isotope excursion (CIE) associated with H2 hyperthermal, yellow shaded region (DEV2) indicates CIE associated with ETM2, and blue shaded region (DEV1) indicates the ^{2}H-enriched interval. Analytical uncertainty is based on precision of external standards, which is larger than standard deviations for replicate analysis. Propagated Percentage Error (PPE, %) for ACL-predicted δ^2H is calculated from difference between the observed and predicted δ^2H (using the relationship in Fig. 2a). Uncertainty shown in Fig. 2b is the mean PPE for all estimates, with a confidence interval of 95%. (For interpretation of the references to color in this figure legend, the reader is referred to the web version of this article.)

transport (e.g. Lena and Yana river drainage areas; Martinez et al., 2009), during the Late Paleocene and early Eocene, with increased aquatic input during hyperthermal events (Boucsein and Stein, 2009). Evidence for greater organic matter burial during the PETM and ETM2 is accompanied by low values in the detrital heavy mineral fraction (Ti/Al, Zr/Al) and slight enrichments in redox-sensitive sulfide-forming elements, suggesting oxygen-deficient and less agitated bottom water masses (Marz et al., 2010). Other evidence for enhanced river discharge during the Eocene comes from radiolarian and terrestrial palynomorph data (Backman et al., 2006) and from dinocysts assemblages that show a reduction in marine dinocysts and an increase in low-salinity tolerant dinocysts coinciding with pre-CIE ^{2}H-enrichment (Sluijs et al., 2009; Fig. 2). Thus, a range of data support changes in fluvial fluxes or spatial distribution of fluvial input prior to the hyperthermals. ^{2}H-enrichment during DEV1 also supports a period of climate shift or environmental change prior to the CIE (Sluijs et al., 2007). Indeed, TEX_{86} records indicate colder, rather than warmer high-latitude temperatures during this interval (Fig. 3), which would have increased the meridional temperature gradient and shifted δ^2H of precipitation to more negative values. However, we observe ^{2}H-enrichment at the North Pole during this time.

DEV2 represents a rapid negative $\delta^2H_{n\text{-alkane}}$ excursion near the base of the CIE (Fig. 2b). Assuming this interval reflects the base of rapid warming and greenhouse-gas input, a simple Rayleigh distillation model with reduced meridional temperature gradient would predict the opposite behavior than what is observed. That is, global warming is expected to lead to ^{2}H-enriched precipitation in the Arctic due to reduced meridional rainout during poleward vapor transport. In general, precipitation at higher latitudes derives from waters evaporated in the sub-tropics (Held and Soden, 2006). Poleward moisture transport and precipitation results in an increase of lighter isotopes in the vapor and condensate. Thus, our results are not consistent with the classic hydrological cycle paradigm, which would require an increase in the δ^2H value of high latitude precipitation with an increase in the vigor of the hydrological cycle.

DEV3 occurs during the presumed H2 hyperthermal event (Fig. 2b) — the hyperthermal that follows ETM2 (Stap et al., 2010). H2 was not positively identified at the study site. Sluijs et al. (2009) suggested its presence based on a negative CIE in total organic carbon. This CIE was, however, not reproduced in marine biomarkers suggesting the TOC record was influenced by varying organic matter sourcing (Schoon et al., 2011). A modeling effort to disentangle marine and terrestrial organic matter subsequently suggested the presence of CIE in marine organic matter (Sluijs and Dickens, 2012) but the presence of H2 is not unequivocal. The TEX_{86} record shows no signs of warming but this could be due to vertical migrations of Thaumarcheota — the producers of membrane lipids on which TEX_{86} is based — within the water column due to euxinic conditions developed during the event (Sluijs et al., 2009). The palynological response, notably the increase in abundance of low-salinity tolerant dinoflagellate cysts, is consistent with a hyperthermal. Further, DEV3 is characterized by a strong deviation between ACL and δ^2H trends. Offsets during this interval could reflect true changes in $\delta^2H_{precipitation}$ corresponding to a pre-event ^{2}H-enrichment. However, reworking of older leaf waxes cannot be ruled out and we were not able to evaluate if a negative CIE in $\delta^{13}C_{n\text{-alkane}}$ is present because of low *n*-alkane abundance.

4.3. Mechanisms for observed $^2H/^1H$ changes during ETM2

Explaining our observed isotopic changes in relationship to temperature records and broadly accepted patterns of global temperature change during ETM2 is particularly challenging. Changes in isotopic composition of precipitation, determined by atmospheric temperature and its absolute humidity, is usually conceptualized using a simple Rayleigh isotope distillation model, where ^{2}H-depleted values are predicted at colder temperatures in the higher latitudes due to the decreasing size of the atmospheric vapor reservoir with meridional vapor transport. With global warming, atmospheric moisture content is theoretically predicted (via the Clausius–Clayperon relation) to increase at the rate of ~7%/K, although models and theory of future warming scenarios suggest that global evaporation/precipitation increase at a slower rate of ~3%/K (Held and Soden, 2006). If proportionately lower rainout occurred from a larger vapor reservoir, then a Rayleigh distillation model would predict substantially more positive δ^2H values in the high latitudes. However, this is not observed for the PETM (Pagani et al., 2006) or ETM2 (DEV2) during peak warming. On the contrary, *n*-alkanes suggest that precipitation was slightly more ^{2}H-depleted during the warmth of the hyperthermals (Fig. 1), suggesting that other mechanisms were in play that altered the

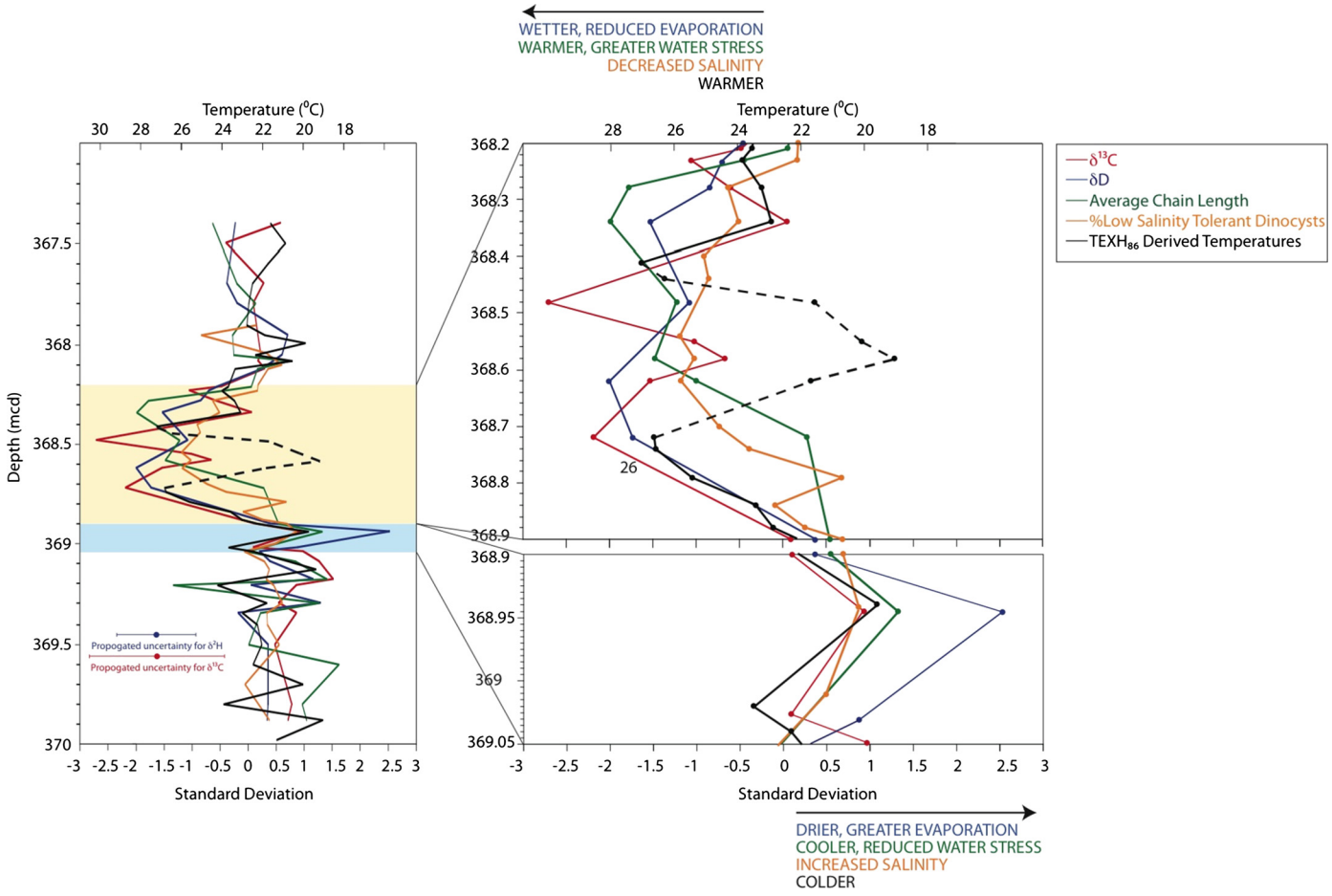

Fig. 3. Changes in TEX_{86}^{H}-derived surface temperatures and standardized anomalies in $\delta^{13}C$, $\delta^{2}H$, average chain length (ACL), percentage-low salinity tolerant dinocysts during Eocene Thermal Maximum 2 (ETM2). Right panels are zoomed in to intervals of interest. The top panel associated with the negative carbon isotope excursion (CIE), and the bottom panel indicates the ^{2}H-enriched interval.

relationship between temperature and isotopic composition of precipitation under different climate states. Given the magnitude of warmth and associated vapor content during the Eocene and hyperthermals, we expect a modification of the vertical structure of the paleoatmosphere, similar to changes observed for future scenarios (Trenberth, 2011). Whether this alters the fraction of vapor involved in long-range transport and rainout processes remains uncertain. Given this uncertainty, our approach is to simply interpret biomarker $^{2}H/^{1}H$ isotopic changes assuming that the size of the atmospheric vapor reservoir (as it pertains to the Rayleigh distillation model) increases at the same rate as global evaporation/precipitation rate.

To infer changes in the climate and environmental state during ETM2, we evaluate carbon and hydrogen isotopic records and ACL values generated here with published temperature and salinity (i.e., low-salinity dinocysts) records (Sluijs et al., 2009). Although these different datasets are related, they are not strictly comparable; i.e. the spread within each dataset can result in misleading interpretations. To overcome these uncertainties, we normalize the datasets and evaluate standardized anomalies (Wilks, 1995). The standardized anomaly is calculated by subtracting the sample mean from the raw values and dividing the anomaly by the corresponding standard deviation (Eq. (3)).

$$z = \frac{x - \overline{X}}{s} \tag{3}$$

where z is the calculated standardized anomaly for each variable; x is the measured value; $\overline{X}$ is the mean value for the dataset; s is the standard deviation. In this way, variability of different datasets can be examined on the same scale in order to develop conceptual models that explain their observed shifts.

Interestingly, standardized anomalies of all five records broadly co-vary through the climate perturbation (Fig. 3) and suggest that changes reflect uniform shifts in the environment and climate of the high Arctic. During DEV1, ^{2}H-enrichment is accompanied by a decrease in the percentage of low salinity-tolerant dinocysts and lower TEX_{86}^{H}-derived temperatures, implying cooler and more saline environments (e.g., reduced fluvial discharge) prior to ETM2. Within the CIE, all records uniformly shift, suggesting a switch to a different regional climate/environmental regime — a warmer, wetter climate with an input of fresh surface waters, similar to changes determined for the PETM. Within the body of the ETM2, TEX_{86}^{H}-temperatures imply a period of SST cooling. Whether or not local cooling was an artifact of the proxy measurement is not entirely clear. Sluijs et al. (2009) argued that lower temperatures potentially reflect the migration of GDGT-producing archaea to deeper depths of the chemocline. Euxinic photic-zone conditions during this interval are supported by an increase in abundance of the biomarker isorenieratane, produced by photosynthetic green sulfur bacteria (Sluijs et al., 2009). However, we also observe a positive shift in $\delta^{13}C_{n\text{-alkane}}$ at the same interval, suggesting a broader environmental response. Perhaps these shifts reflect a transient drop in greenhouse levels and colder temperatures in the middle of the hyperthermal. Similar shifts in marine biomarker $\delta^{13}C$ (Schoon et al., 2011) were argued to reflect an increase in primary productivity that would increase growth rate and biomarker

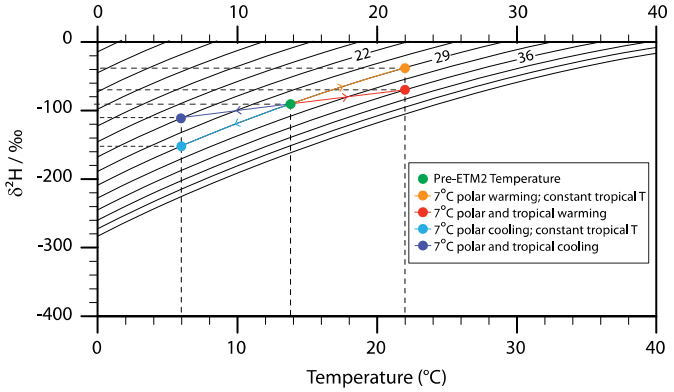

Fig. 4. Simple Rayleigh Distillation Model. Equilibrium vapor pressure used to calculate f was estimated using $(3.69\text{E}{-7} + 1.53\text{E}{-9} * (T - 15) - 5.41\text{E}{-11} * (T - 15)^2 + 5.35\text{E}{-16} * (T - 15)^3 - 1.28\text{E}{-13} * (T - 15)^4) * \exp(0.062300128260019 * (T + 273.16))$. Temperature dependance of α is calculated after Dansgaard (1964). Contour lines indicate δ^2H values for different initial equilibration (tropical; marked on the contour) and polar temperatures.

abundance while decreasing isotopic fractionation. However, this mechanism cannot explain observed changes in $\delta^{13}C_{n\text{-alkanes}}$. It is likely that the positive shift in $\delta^{13}C_{n\text{-alkane}}$ reflect local effects, such as changes in runoff or ocean stratification that result in reworking of older (i.e., pre-event) leaf waxes during peak warming.

In sum, our analysis indicates that isotopic shifts occurred in relation to environmental perturbations, and that warming is clearly associated with isotopic depletion and cooling with D-enrichment. The occurrence of ^{2}H-enriched *n*-alkanes prior to the onset of ETM2 (coeval with the colder temperatures) followed by ^{2}H-depleted signals during peak warming is identical to patterns and relationships observed for the Arctic PETM (Pagani et al., 2006). Similar trends in ^{2}H/^{1}H changes (with smaller magnitudes) are also recorded at midlatitude PETM sites, including the Big-Horn Basin (Smith et al., 2007) and Forada, Italy (Tipple and Pagani, 2012).

In general, these relationships defy simple Rayleigh distillation scenarios, such as the predictions of Pagani et al. (2006). Discrepancy between theory and observations could result if: (1) the available high latitude temperature records represent a localized signal and are not indicative of broad regional temperatures. Indeed, pre-CIE cooling trends in TEX_{86} temperature records have been observed in the Arctic (Fig. 4, Sluijs et al., 2006), and Antarctic (Sluijs et al., 2011) for the PETM. Therefore, a short period of pre-event high latitude cooling prior to the CIE cannot be rejected, or (2) an alternative atmospheric mechanism is at play that alters ^{2}H/^{1}H compositions of high latitude meteoric water, but does not follow a simple Rayleigh distillation model.

We consider three scenarios that could help explain the observed isotopic relationships: (1) regional changes in E/P with equatorward vapor return flow, (2) extratropical storms and high latitude amount effects, and (3) temperature changes at the low-latitudes.

4.4. Regional changes in E/P with equatorward vapor return flow

For DEV1, intensification of local surface/soil water evaporation, as indicated by evidence for reduced runoff and more saline surface waters (Fig. 3; Sluijs et al., 2009) and drying over land would have ^{2}H-enriched local meteoric water. In contrast, more negative $\delta^2H_{n\text{-alkane}}$ values during the body of ETM2 (i.e., DEV2) suggest a local reduction in evaporation, with a warm and wet environment, supported by other evidence (Sluijs et al., 2009). However, similar ^{2}H-enrichment observed in the midlatitudes (Tipple et al., 2011) requires a mechanism that links isotopic shifts in the mid- and high-latitudes. The Rayleigh distillation model is unidirectional and assumes evaporation occurs in the sub-tropics with poleward vapor transport. Conditions during the warmth of the Eocene and hyperthermals could have been distinctly different. For example, Noone (2008) suggested that the addition of water vapor due to surface evaporation during equator-ward return flow could play an important role in setting the isotopic composition of meteoric water at midlatitudes. Given extraordinarily warm high latitudes during the Eocene, a moist equator-ward return flow could have led to ^{2}H-depleted midlatitude precipitation, mirroring high-latitude precipitation. Existing proxies do not allow for an adequate evaluation of the degree of surface evaporation or the moistness of the equatorward return-flow in order to test this supposition.

4.5. Extratropical storms and high latitude amount effects

Observations in the modern tropics and sub-tropics indicate that the isotopic composition of precipitation is related to the precipitation rate, rather than air temperature (Rozanski et al., 1993; Gat, 1996). Termed the 'amount effect', Dansgaard (1964) suggested that this relationship is the result of the removal of heavy isotopologues as the clouds cool. Alternatively, Bony et al. (2008) and Risi et al. (2008) assessed microphysical processes during convection and suggested that this effect is driven by unsaturated downdrafts — during intense convection, higher precipitation rates and sub-cloud relative humidity would result in reduced evaporative enrichment and increasingly ^{2}H-depleted rainout. Similarly, intense precipitation events are also associated with larger droplet size and incomplete isotopic equilibration of the raindrops with ambient vapor, leading to ^{2}H-depleted precipitation. During the extreme warmth of the Eocene, the expression and intensity of extratropical storms and isotopic perturbations related to 'amount effects' associated with tropical storms today could have been common across the high latitudes. Under future warming scenarios, modeling studies have suggested a poleward shift in storm tracks and an increase in the intensity of extreme events (Held and Soden, 2006; Mizuta et al., 2011). This hypothesis is supported by evidence for increased seasonality and storms during the PETM (Schmitz and Pujalte, 2007; Wing et al., 2005; Eldrett et al., 2014). Conversely, cooler temperatures prior to the CIE would be associated with less intense storm events, resulting in a smaller 'amount effect' and more positive $\delta^2H_{n\text{-alkanes}}$ values. Compared to the midlatitudes, this effect would be amplified at the high latitudes and result in larger $^2H/^1H_{precipitation}$ shifts. Testing this supposition will require expanding high-resolution hyperthermal records across the midlatitudes.

4.6. Changes in low latitude temperatures

Today, greenhouse-gas induced warming reduces the meridional temperature gradient due to polar amplification. However in the ice-free world of the early Eocene, it is possible that polar amplification and meridional temperature gradients were greatly different (Barron, 1987; Caballero and Langen, 2005; Sluijs et al., 2006). Moreover, there is a poor understanding of how tropical temperatures changed during the hyperthermals. Since the majority of water vapor today is sourced from the tropics, it is possible that global changes in ^{2}H/^{1}H ratios were a consequence of changing low-latitude temperatures. Tropical temperatures can affect ^{2}H/^{1}H ratios either by modifying the initial equilibration temperatures (Boyle, 1997) or by changing the meridional temperature gradient/rainout fraction. High latitude warming results in ^{2}H-enrichment, while coeval tropical warming attenuates the magnitude of high-latitude ^{2}H-enrichment (Fig. 4). Similar magnitudes of warming in the tropics and high latitudes with little to

no change in the meridional temperature gradient leads to high-latitude ^{2}H-enrichment. Therefore, changes in the initial equilibration temperature alone cannot explain the observed isotopic structure during the hyperthermals. If changes in isotopic distillation is solely responsible for observed ^{2}H/^{1}H shifts, then observed records indicate that the tropics had to warm by a greater degree than the Arctic during the hyperthermals.

Pre-event ^{2}H-enrichments can result either from uniform global warming prior to the CIE (not supported by the TEX_{86} record at the Arctic) or by cooling the tropics more than the Arctic (Fig. 4). Since neither of these mechanisms appears plausible for hyperthermal conditions, we reject the hypothesis that changes in low-latitude temperatures caused pre-event Arctic ^{2}H-enrichments.

In summary, it is clear that similar patterns of hydrological change in the Arctic are observed during the early Eocene hyperthermals. Available evidence indicates pre-event hydrological changes and fundamental shifts in the climate system prior to the CIE. TEX_{86}-derived surface temperature records from the Arctic indicate colder temperatures prior to the hyperthermals, accompanied by significant ^{2}H-enrichment in $\delta^2H_{n\text{-alkane}}$ values. Distinguishing whether these changes reflect regional changes in E/P or in the frequency and intensity of extra-tropical storm activity requires proxies that can either quantify high-latitude evaporation or extra-tropical storm activity with warming. Regardless, it is possible that the factors that promoted hydrological change played a key role in the release of greenhouse gases responsible for global warming. For example, colder high-latitude environments immediately preceding the CIE would have fostered the expansion of high-latitude permafrost carbon reservoirs at high elevation (DeConto et al., 2012). Increased local evaporation from soils could have also lowered ground water levels, leading to drier soils, increased peat oxidation. Ultimately, determining causal links between the hydrological cycle and high-latitude temperatures will be instrumental in constraining the source and mechanism of carbon release that triggered the early Eocene hyperthermals. Further, we suggest that large ^{2}H-depletion during peak CIE for both hyperthermals point to substantial changes in Arctic hydrology with rapid warming. Models have traditionally been poor in replicating the low meridional temperature gradient observed in proxy records for the early Eocene and peak PETM conditions (Lunt et al., 2012). Isotopic evidence for increased meridional temperature gradient (i.e. increased ^{2}H-depletion) during the body of the hyperthermals point to two potential reasons for observed discrepancy in data-model comparisons, (1) lack of available low-latitude temperature records or (2) inadequate model description of high-latitude hydrological cycle and associated feedbacks.

5. Conclusion

Comparison of ^{2}H/^{1}H trends in Arctic biomarker records for two different hyperthermal events during the early Eocene suggest similar changes in the hydrological cycle concomitant with warming. Both hyperthermals are associated with ^{2}H-enrichments of leaf-wax lipids (+60‰ during the PETM and +20‰ during ETM2) prior to the negative CIE. The timing of ^{2}H-enrichment suggests high latitude climatic or environmental changes preceded the massive release of carbon that characterizes the hyperthermals (Sluijs et al., 2007). Understanding the nature and reasons for these hydrological shifts are more complex. In contrast to early assertions that ^{2}H-enrichment resulted from reduced midlatitude rainout and increased poleward moisture transport with warming, a more detailed record of ETM2 indicates that ^{2}H-enrichment prior to the CIE was associated with colder temperatures and do not reflect changes in vegetation or *n*-alkane sources. Therefore, $\delta^2H_{n\text{-alkane}}$ shifts likely reflect changes in precipitation ^{2}H/^{1}H compositions that cannot be explained by changes in meridional temperature gradients. Three potential scenarios that can help explain isotopic shifts observed at high and midlatitudes are suggested and include (1) changes in the rates of local evapotranspiration or soil evaporation and its influence on local meteoric water signals, coupled with equator-ward vapor transport, (2) high latitude 'amount effects' due to convective upwelling and intense storm activity, and finally, (3) changes in tropical temperatures that influence initial isotopic composition of vapor and the meridional temperature gradient. Using simple Rayleigh distillation models, we reject the plausibility of scenario 3.

Acknowledgements

We thank two anonymous reviewers and S. Feakins for constructive comments that resulted in significant improvements to the manuscript. This research was supported by the National Science Foundation Grants #0902993 and #0628719 awarded to Mark Pagani, National Science Foundation P2C2 Grant OCE #0902882 awarded to Matthew Huber, and Schlanger Ocean Drilling Fellowship (part of the NSF sponsored U.S. Science Support Program; USSSP) for the year 2008–2009 awarded to Srinath Krishnan. Additional funding for this research was provided to Appy Sluijs by the Netherlands Organization for Scientific Research (Veni grant 863.07.001) and the European Research Council under the European Community's Seventh Framework Program (ERC Starting Grant #259627). All isotope analyses were performed at the Yale Institute for Biospheric Studies–Earth Systems Center for Stable Isotopic Studies.

References

Abels, H.A., Clyde, W.C., Gingerich, P.D., Hilgen, F.J., Fricke, H.C., Bowen, G.J., Lourens, L.J., 2012. Terrestrial carbon isotope excursions and biotic change during Palaeogene hyperthermals. Nat. Geosci. 5.

Allan, R.P., Soden, B.J., 2007. Large discrepancy between observed and simulated precipitation trends in the ascending and descending branches of the tropical circulation. Geophys. Res. Lett. 34, 1–6.

Allen, R.M., Ingram, W.J., 2002. Constraints on future changes in climate and the hydrological cycle. Nature 419, 224–232.

Andersen, N., Paul, H.A., Bernasconi, S.M., McKenzie, J.A., Behrens, A., Schaeffer, P., Albrecht, P., 2001. Large and rapid climate variability during the Messinian salinity crisis: evidence from deuterium concentrations of individual biomarkers. Geology 29 (9), 799–802.

Backman, J., Moran, K., McInroy, D.B., Mayer, L.A., Expedition 302 Scientists, 2006. Proceedings of the Integrated Ocean Drilling Program, 302. Integrated Ocean Drilling Program Management International, Inc., College Station, TX.

Barron, Eric J., 1987. Eocene equator-to-pole surface ocean temperatures: a significant climate problem? Paleoceanography 6, 729–739.

Barron, E., Hay, W., Thompson, S., 1989. The hydrologic cycle: a major variable during Earth history. Palaeogeogr. Palaeoclimatol. Palaeoecol. 75, 157–174.

Bi, X., Sheng, G., Liu, X., Li, C., Fu, J., 2005. Molecular and carbon and hydrogen isotopic composition of *n*-alkanes in plant leaf waxes. Org. Geochem. 36, 1405–1417.

Bony, S., Risi, C., Vimeux, F., 2008. Influence of convective processes on the isotopic composition (δ^{18}O and δD) of precipitation and water vapor in the tropics: 1. Radiative–convective equilibrium and Tropical Ocean-Global Atmosphere-Coupled Ocean-Atmosphere Response Experiment (TOGA-COARE). J. Geophys. Res. 113, 1–21.

Boucsein, B., Stein, R., 2009. Black shale formation in the late Paleocene/early Eocene Arctic Ocean and paleoenvironmental conditions: new results from a detailed petrological study. Mar. Pet. Geol. 26, 416–426.

Bowen, G., Beerling, D., Koch, P., Zachos, J., Quattlebaum, T., 2004. A humid climate state during the Palaeocene/Eocene thermal maximum. Nature 432, 495–499.

Boyle, E.A., 1997. Cool tropical temperatures shift the global δ^{18}O–T relationship: an explanation for the ice core δ^{18}O – borehole thermometry conflict? Geophys. Res. Lett. 24, 273–276.

Bralower, T.J., Thomas, D.J., Zachos, J.C., Hirschmann, M.M., Rohl, U., Sigurdsson, H., Thomas, E., Whitney, D.L., 1997. High-resolution records of the late Paleocene thermal maximum and circum-Caribbean volcanism: is there a causal link? Geology 25, 963–966.

Bush, R.T., McInerney, F.A., 2013. Leaf wax n-alkane distributions in and across modern plants: implications for paleoecology and chemotaxonomy. Geochem. Cosmochim. Acta 117, 161–179.

Caballero, R., Langen, L.P., 2005. The dynamic range of poleward energy transport in an atmospheric general circulation model. Geophys. Res. Lett. 32, L02705.
Chikaraishi, Y., Naraoka, H., 2003. Compound-specific δD–δ^{13}C analyses of *n*-alkanes extracted from terrestrial and aquatic plants. Phytochemistry 63, 361–371.
Conte, M., Weber, J., 2002. Long-range atmospheric transport of terrestrial biomarkers to the western North Atlantic. Glob. Biogeochem. Cycles 16, 1142.
Cramer, B.S., Wright, J.D., Kent, D.V., Aubry, M.P., 2003. Orbital climate forcing of δ^{13}C excursions in the late Paleocene–early Eocene (chrons C24n–C25n). Paleoceanography 18 (4).
Crouch, E.M., Dickens, G.R., Brinkhuis, H., Aubry, M.P., Hollis, C.J., Rogers, K.M., Visscher, H., 2003. The Apectodinium acme and terrestrial discharge during the Paleocene–Eocene thermal maximum: new palynological, geochemical and calcareous nannoplankton observations at Tawanui, New Zealand. Palaeogeogr. Palaeoclimatol. Palaeoecol. 194 (4), 387–403.
Dansgaard, W., 1964. Stable isotopes in precipitation. Tellus 16, 436–468.
de Leeuw, J.W., Frewin, N.L., Van Bergen, P.F., Damste, J.S.S., Collinson, M.E., 1995. Organic carbon as a palaeoenvironmental indicator in the marine realm. Geol. Soc. (Lond.) Spec. Publ. 83, 43–71.
DeConto, R.M., Galeotti, S., Pagani, M., Tracy, D., Schaefer, K., Zhang, T., Pollard, D., Beerling, D.J., 2012. Past extreme warming events linked to massive carbon release from thawing permafrost. Nature 484, 87–91.
Dickens, G.R., O'Neil, J.R., Rea, D.K., Owen, R.M., 1995. Dissociation of oceanic methane hydrate as a cause of the carbon isotope excursion at the end of the Paleocene. Paleoceanography 10, 965–971.
Dickens, G.R., Castillo, M.M., Walker, J.C.G., 1997. A blast of gas in the latest Paleocene: simulating first-order effects of massive dissociation of oceanic methane hydrate. Geology 25, 259–262.
Diefendorf, A.F., Freeman, K.H., Wing, S.L., Graham, H.V., 2011. Production of *n*-alkyl lipids in living plants and implications for the geologic past. Geochim. Cosmochim. Acta 75, 7472–7485.
Douglas, M.J., Pagani, M., Brenner, M., Hodell, D.A., Curtis, J.H., 2012. Aridity and vegetation composition are important determinants of leaf-wax δD values in southeastern Mexico and Central America. Geochim. Cosmochim. Acta 97, 24–45.
Dunkley Jones, T., Lunt, D.J., Schmidt, D.N., Ridgwell, A., Sluijs, A., Valdes, P.J., Maslin, M., 2013. Climate model and proxy data constraints on ocean warming across the Paleocene–Eocene Thermal Maximum. Earth-Sci. Rev. 125, 123–145.
Eldrett, J.S., Greenwood, D.R., Polling, M., Brinkhuis, H., Sluijs, A., 2014. A seasonality trigger for carbon injection at the Paleocene–Eocene Thermal Maximum. Clim. Past 10 (2), 759–769.
Feakins, S.J., 2013. Pollen-corrected leaf wax D/H reconstructions of northeast African hydrological changes during the late Miocene. Palaeogeogr. Palaeoclimatol. Palaeoecol. 374, 62–71.
Feakins, S., Sessions, A., 2010. Controls on the D/H ratios of plant leaf waxes in an arid ecosystem. Geochim. Cosmochim. Acta 74 (7), 2128–2141.
Feakins, S.J., Warny, S., Lee, J.E., 2012. Hydrologic cycling over Antarctica during the middle Miocene warming. Nat. Geosci. 5 (8), 557–560.
Galeotti, S., Krishnan, S., Pagani, M., Lanci, L., Gaudio, A., Zachos, J.C., Monechi, S., Morelli, G., Lourens, L., 2010. Orbital chronology of early Eocene hyperthermals from the Contessa Road section, central Italy. Earth Planet. Sci. Lett. 290, 192–200.
Gat, J.R., 1996. Oxygen and hydrogen isotopes in the hydrologic cycle. Annu. Rev. Earth Planet. Sci. 24, 225–262.
Giusberti, L., Rio, D., Agnini, C., Backman, J., Fornaciari, E., Tateo, F., Oddone, M., 2007. Mode and tempo of the Paleocene–Eocene thermal maximum in an expanded section from the Venetian pre-Alps. Geol. Soc. Am. Bull. 119 (3–4), 391–412.
Handley, L., Pearson, P.N., McMillan, I.K., Pancost, R.D., 2008. Large terrestrial and marine carbon and hydrogen isotope excursions in a new Paleocene/Eocene boundary section from Tanzania. Earth Planet. Sci. Lett. 275, 17–25.
Handley, L., O'Halloran, A., Pearson, P.N., Hawkins, E., Nicholas, C.J., Schouten, S., Mcmillan, I.K., Pancost, R.D., 2012. Changes in the hydrological cycle in tropical East Africa during the Paleocene–Eocene Thermal Maximum. Palaeogeogr. Palaeoclimatol. Palaeoecol. 329 (220), 10–21.
Harding, I.C., Charles, A.J., Marshall, J.E.A., Pälike, H., Roberts, A.P., Wilson, P.A., Jarvis, E., Thorne, R., Morris, E., Moremon, R., Pearce, R.B., Akbari, S., 2011. Sea-level and salinity fluctuations during the Paleocene–Eocene thermal maximum in Arctic Spitsbergen. Earth Planet. Sci. Lett. 303 (1–2), 97–107. http://dx.doi.org/10.1016/j.epsl.2010.12.043.
Held, I.M., Soden, B.J., 2006. Robust responses of the hydrological cycle to global warming. J. Climate 19, 5686–5699.
Higgins, J., Schrag, D., 2006. Beyond methane: towards a theory for the Paleocene–Eocene thermal maximum. Earth Planet. Sci. Lett. 245, 523–537.
Hollis, C.J., Dickens, G.R., Field, B.D., Jones, C.M., Strong, C.P., 2005. The Paleocene–Eocene transition at Mead Stream, New Zealand: a southern Pacific record of early Cenozoic global change. Palaeogeogr. Palaeoclimatol. Palaeoecol. 215 (3/4), 313–343.
Hopmans, E.C., Weijers, J.W., Schefuß, E., Herfort, L., Sinninghe Damsté, J.S., Schouten, S., 2004. A novel proxy for terrestrial organic matter in sediments based on branched and isoprenoid tetraether lipids. Earth Planet. Sci. Lett. 224 (1), 107–116.
Hou, J., D'Andrea, W.J., MacDonald, D., Huang, Y., 2007. Hydrogen isotopic variability in leaf waxes among terrestrial and aquatic plants around Blood Pond, Massachusetts (USA). Org. Geochem. 38, 977–984.
Huang, Y., Lockheart, M.J., Collister, J.W., Eglinton, G., 1995. Molecular and isotopic biogeochemistry of the Miocene Clarkia formation: hydrocarbons and alcohols. Org. Geochem. 23, 785–801.
Huang, Y., Dupont, L., Sarnthein, M., Hayes, J.M., Eglinton, G., 2000. Mapping of C4 plant input from North West Africa into North East Atlantic sediments. Geochim. Cosmochim. Acta 64, 3505–3513.
Huang, Y., Shuman, B., Wang, Y., Webb, T., 2002. Hydrogen isotope ratios of palmitic acid in lacustrine sediments record late Quaternary climate variations. Geology 30, 1103–1106.
Huber, M., 2009. Climate change: snakes tell a torrid tale. Nature 457 (7230), 669–671.
Huber, M., Caballero, R., 2011. The early Eocene equable climate problem revisited. Clim. Past 7, 603–633.
Huntington, T.G., 2006. Evidence for intensification of the global water cycle: review and synthesis. J. Hydrol. 319, 83–95.
Jaramillo, C., Ochoa, D., Contreras, L., Pagani, M., Carvajal-Ortiz, H., Pratt, L.M., Krishnan, S., Cardona, A., Romero, M., Quiroz, L., Rodriguez, G., Rueda, M.J., de la Parra, F., Moron, S., Green, W., Bayona, G., Montes, C., Quintero, O., Ramirez, R., Mora, G., Schouten, S., Bermudez, H., Navarrete, R., Parra, F., Alvaran, M., Osorno, J., Crowley, J.L., Valencia, V., Vervoort, J., 2010. Effects of rapid global warming at the Paleocene–Eocene boundary on neotropical vegetation. Science 330, 957–961.
Kennett, J.P., Stott, L.D., 1991. Abrupt deep-sea warming, paleoceanographic changes and benthic extinctions at the end of the Paleocene. Nature 353, 225–228.
Kent, D.V., Cramer, B.S., Lanci, L., Wang, D., Wright, J.D., Van der Voo, R., 2003. A case for a comet impact trigger for the Paleocene/Eocene thermal maximum and carbon isotope excursion. Earth Planet. Sci. Lett. 211 (1), 13–26.
Knies, J., Mann, U., Popp, B.N., Stein, R., Brumsack, H.J., 2008. Surface water productivity and paleoceanographic implications in the Cenozoic Arctic Ocean. Paleoceanography 23 (1).
Koch, P.L., Zachos, J.C., Gingerich, P.D., 1992. Correlation between isotope records in marine and continental carbon reservoirs near the Palaeocene/Eocene boundary. Nature 358, 319–322.
Kurtz, A.C., 2003. Early Cenozoic decoupling of the global carbon and sulfur cycles. Paleoceanography 18. http://dx.doi.org/10.1029/2003PA000908.
Lourens, L.J., Sluijs, A., Kroon, D., Zachos, J.C., Thomas, E., Rohl, U., Bowles, J., Raffi, I., 2005. Astronomical pacing of late Palaeocene to early Eocene global warming events. Nature 435, 1083–1087.
Lunt, D.J., Ridgwell, A., Sluijs, A., Zachos, J., Hunter, S., Haywood, A., 2011. A model for orbital pacing of methane hydrate destabilization during the Palaeogene. Nat. Geosci. 4 (11), 775–778.
Lunt, D.J., Dunkley Jones, T., Heinemann, M., Huber, M., LeGrande, A., Winguth, A., Loptson, C., Marotzke, J., Roberts, C.D., Tindall, J., Valdes, P., Winguth, C., 2012. A model–data comparison for a multi-model ensemble of early Eocene atmosphere–ocean simulations: EoMIP. Clim. Past 8, 1717–1736.
Martinez, N.C., Murray, R.W., Dickens, G.R., Kölling, M., 2009. Discrimination of sources of terrigenous sediment deposited in the central Arctic Ocean through the Cenozoic. Paleoceanography 24, PA1210.
März, C., Schnetger, B., Brumsack, H.J., 2010. Paleoenvironmental implications of Cenozoic sediments from the central Arctic Ocean (IODP Expedition 302) using inorganic geochemistry. Paleoceanography 25, PA3206.
Mizuta, R., Matsueda, M., Endo, H., Yukimoto, S., 2011. Future change in extratropical cyclones associated with change in the upper troposphere. J. Climate 24, 6456–6470.
Nicolo, M.J., Dickens, G.R., Hollis, C.J., Zachos, J.C., 2007. Multiple early Eocene hyperthermals: their sedimentary expression on the New Zealand continental margin and in the deep sea. Geology 35 (8), 699–702.
Noone, D., 2008. The influence of midlatitude and tropical overturning circulation on the isotopic composition of atmospheric water vapor and Antarctic precipitation. J. Geophys. Res., Atmos. (1984–2012) 113, D4.
NRC (National Research Council), 2006. Surface Temperature Reconstructions for the Last 2,000 Year. National Academies Press, Washington, DC.
O'Regan, A., Moran, K., Backman, J., Jakobsson, M., Sangiorgi, F., Brinkhuis, H., Pockalny, R., Skelton, A., Stickley, C., Koc, N., Brumsack, H., Willard, D., 2008. Mid-Cenozoic tectonic and paleoenvironmental setting of the central Arctic Ocean. Paleoceanography 23. http://dx.doi.org/10.1029/2007PA001559.
Pagani, M., Pedentchouk, N., Huber, M., Sluijs, A., Schouten, S., Brinkhuis, H., Damste, J.S.S., Dickens, G.R., Expedition 302 Scientists, 2006. Arctic hydrology during global warming at the Palaeocene/Eocene thermal maximum. Nature 442, 671–675.
Pancost, R.D., Boot, C.S., 2004. The palaeoclimatic utility of terrestrial biomarkers in marine sediments. Mar. Chem. 92, 239–261.
Pedentchouk, N., Freeman, K.H., Harris, N.B., 2006. Different response of δD values of *n*-alkanes, isoprenoids, and kerogen during thermal maturation. Geochim. Cosmochim. Acta 70, 2063–2072.
Pedentchouk, N., Sumner, W., Tipple, B.J., Pagani, M., 2008. δ^{13}C and δD compositions of *n*-alkanes from modern angiosperms and conifers: an experimental set up in central Washington State, USA. Org. Geochem. 39, 1066–1071.

Pierrehumbert, R.T., 2002. The hydrologic cycle in deep-time climate problems. Nature 419 (6903), 191–198.
Polissar, P.J., Freeman, K.H., 2010. Effects of aridity and vegetation on plant-wax δD in modern lake sediments. Geochim. Cosmochim. Acta 74, 5785–5797.
Polissar, P.J., Freeman, K.H., Rowley, D.B., McInerney, F.A., Currie, B.S., 2009. Paleoaltimetry of the Tibetan Plateau from D/H ratios of lipid biomarkers. Earth Planet. Sci. Lett. 287, 64–76.
Risi, C., Bony, S., Vimeux, F., 2008. Influence of convective processes on the isotopic composition (δ^{18}O and δD) of precipitation and water vapor in the tropics: 2. Physical interpretation of the amount effect. J. Geophys. Res. 113, 1–12.
Rozanski, K., Araguás-Araguás, L., Gonfiantini, R., 1993. Isotopic patterns in modern global precipitation. In: Climate Change in Continental Isotopic Records, pp. 1–36.
Sachse, D., Radke, J., Gleixner, G., 2006. δD values of individual *n*-alkanes from terrestrial plants along a climatic gradient – implications for the sedimentary biomarker record. Org. Geochem. 37, 469–483.
Sachse, D., Billault, I., Bowen, G.J., Chikaraishi, Y., Dawson, T.E., Feakins, S.J., Freeman, K.H., Magill, C.R., McInerney, F.A., van der Meer, M.T.J., Polissar, P.J., Robins, R.J., Sachs, J.P., Schmidt, H.-L., Sessions, A.L., White, J.W.C., West, J.B., Kahmen, A., 2012. Molecular paleohydrology: interpreting the hydrogen-isotopic composition of lipid biomarkers from photosynthesizing organisms. Annu. Rev. Earth Planet. Sci. 40 (1), 221–249.
Schefuß, E., Kuhlmann, H., Mollenhauer, G., Prange, M., Pätzold, J., 2011. Forcing of wet phases in southeast Africa over the past 17,000 years. Nature 480 (7378), 509–512.
Schmitz, B., Pujalte, V., 2007. Abrupt increase in seasonal extreme precipitation at the Paleocene–Eocene boundary. Geology 35, 215–218.
Schmitz, B., Speijer, R.P., Aubry, M.-P., 1996. Latest Paleocene benthic extinction event on the southern Tethyan shelf (Egypt): foraminiferal stable isotopic (δ^{13}C, δ^{18}O) records. Geology 24, 347–350.
Schoon, P.L., Sluijs, A., Sinninghe Damsté, J.S., Schouten, S., 2011. Stable carbon isotope patterns of marine biomarker lipids in the Arctic Ocean during Eocene Thermal Maximum 2. Paleoceanography 26 (3).
Schoon, P.L., Heilmann-Clausen, C., Pagh Schultz, B., Sluijs, A., Sinninghe Damsté, J.S., Schouten, S., 2013. Recognition of Early Eocene global carbon isotope excursions using lipids of marine Thaumarchaeota. Earth Planet. Sci. Lett. 373, 160–168.
Schouten, S., Ossebaar, J., Schreiber, K., Kienhuis, M.V.M., Langer, G., Benthien, A., Bijma, J., 2006. The effect of temperature, salinity and growth rate on the stable hydrogen isotopic composition of long chain alkenones produced by Emiliania Huxleyi and Gephyrocapsa Oceanica. Biogeosciences 3, 113–119.
Schouten, S., Forster, A., Panoto, F.E., Sinninghe Damsté, J.S., 2007. Towards calibration of the TEX_{86} palaeothermometer for tropical sea surface temperatures in ancient greenhouse worlds. Org. Geochem., 1537–1546.
Slotnick, B.S., Dickens, G.R., Nicolo, M.J., Hollis, C.J., Crampton, J.S., Zachos, J.C., Sluijs, A., 2012. Large-amplitude variations in carbon cycling and terrestrial weathering during the latest Paleocene and earliest Eocene: the record at Mead Stream, New Zealand. J. Geol. 120 (5), 487–505.
Sluijs, A., Brinkhuis, H., 2009. A dynamic climate and ecosystem state during the Paleocene–Eocene Thermal Maximum: inferences from dinoflagellate cyst assemblages on the New Jersey Shelf. Biogeosciences 6 (8), 1755–1781.
Sluijs, A., Dickens, G.R., 2012. Assessing offsets between the δ^{13}C of sedimentary components and the global exogenic carbon pool across early Paleogene carbon cycle perturbations. Glob. Biogeochem. Cycles 26 (4). http://dx.doi.org/10.1029/2011GB004224.
Sluijs, A., Schouten, S., Pagani, M., Woltering, M., Brinkhuis, H., Sinninghe Damsté, J.S., Dickens, G.R., Huber, M., Reichart, G.-J., Stein, R., Matthiessen, J., Lourens, L.J., Pedentchouk, N., Backman, J., Moran, K., 2006. Subtropical Arctic Ocean temperatures and Palaeocene/Eocene thermal maximum. Nature 441, 610–613.
Sluijs, A., Brinkhuis, H., Schouten, S., Bohaty, S.M., John, C.M., Zachos, J.C., Sinninghe Damsté, J.S., Crouch, E.M., Dickens, G.R., 2007. Environmental precursors to light carbon input at the Paleocene/Eocene boundary. Nature 450, 1218–1221.
Sluijs, A., Röhl, U., Schouten, S., Brumsack, H.J., Sangiorgi, F., Damsté, J.S.S., Brinkhuis, H., 2008a. Arctic late Paleocene–early Eocene paleoenvironments with special emphasis on the Paleocene–Eocene thermal maximum (Lomonosov Ridge, Integrated Ocean Drilling Program Expedition 302). Paleoceanography 23 (1).
Sluijs, A., Brinkhuis, H., Crouch, E.M., John, C.M., Handley, L., Munsterman, D., Bohaty, S.M., Zachos, J.C., Reichart, G.-J., Schouten, S., Pancost, R., Damsté, J.S.S., Welters, N.L.D., Lotter, A.F., Dickens, G.R., 2008b. Eustatic variations during the Paleocene–Eocene greenhouse world. Paleoceanography 23, PA4216. http://dx.doi.org/10.1029/2008PA001615.
Sluijs, A., Schouten, S., Donders, T.H., Schoon, P.L., Röhl, U., Reichart, G.J., Sangiorgi, F., Kim, J.-H., Sinninghe Damsté, J.S., Brinkhuis, H., 2009. Warm and wet conditions in the Arctic region during Eocene Thermal Maximum 2. Nat. Geosci. 2, 777–780.
Sluijs, A., Bijl, P.K., Schouten, S., Rohl, U., Reichart, G.-J., Brinkhuis, H., 2011. Southern Ocean warming, sea level and hydrological change during the Paleocene–Eocene Thermal Maximum. Clim. Past 7, 47–61.
Smith, F.A., Freeman, K.H., 2006. Influence of physiology and climate on δD of leaf wax *n*-alkanes from C3 and C4 grasses. Geochim. Cosmochim. Acta 70, 1172–1187.
Smith, F.A., Wing, S.L., Freeman, K.H., 2007. Magnitude of the carbon isotope excursion at the Paleocene–Eocene thermal maximum: the role of plant community change. Earth Planet. Sci. Lett. 262, 50–65.
Stap, L., Sluijs, A., Thomas, E., Lourens, L., 2009. Patterns and magnitude of deep sea carbonate dissolution during Eocene Thermal Maximum 2 and H2, Walvis Ridge, southeastern Atlantic Ocean. Paleoceanography 24 (1). http://dx.doi.org/10.1029/2008PA001655.
Stap, L., Lourens, L.J., Thomas, E., Sluijs, A., Bohaty, S., Zachos, J.C., 2010. High-resolution deep-sea carbon and oxygen isotope records of Eocene Thermal Maximum 2 and H2. Geology 38 (7), 607–610.
Stein, R., Boucsein, B., Meyer, H., 2006. Anoxia and high primary production in the Paleogene central Arctic Ocean: first detailed records from Lomonosov Ridge. Geophys. Res. Lett. 33, 18.
Svenson, H., Planke, S., Malthe-Sorenssen, A., Jamtveit, B., Myklebust, R., Eidem, T.R., Rey, S.S., 2004. Release of methane from a volcanic basin as a mechanism for initial Eocene global warming. Nature 429, 524–527.
Thomas, E., Zachos, J.C., 2000. Was the late Paleocene Thermal Maximum a unique event? Gff 122 (1), 169–170.
Thomas, D.J., Bralower, T.J., Zachos, J.C., 1999. New evidence for subtropical warming during the late Paleocene thermal maximum: stable isotopes from Deep Sea Drilling Project Site 527, Walvis Ridge. Paleoceanography 14, 561–570.
Tierney, J.E., Oppo, D.W., Rosenthal, Y., Russell, J.M., Linsley, B.K., 2010. Coordinated hydrological regimes in the Indo-Pacific region during the past two millennia. Paleoceanography 25, PA1102.
Tipple, B., Pagani, M., 2012. Environmental control on eastern broadleaf forest species leaf wax distributions and D/H ratios. Geochim. Cosmochim. Acta 111, 64–77.
Tipple, B., Pagani, M., Krishnan, S., Dirghangi, S., Galeotti, S., Agnini, A., Guisberti, L., Rio, D., 2011. Coupled high-resolution marine and terrestrial records of carbon and hydrologic cycles variations during the Paleocene–Eocene Thermal Maximum (PETM). Earth Planet. Sci. Lett. 311 (1–2), 82–92.
Trenberth, K.E., 2011. Changes in precipitation with climate change. Clim. Res. 47, 123–138.
Wakeham, S.G., Pease, T.K., 1992. Lipid Analysis in Marine Particles and Sediment Samples. Skidaway Institute of Oceanography.
Wentz, F.J., Ricciardulli, L., Hilburn, K., Mears, C., 2007. How much more rain will global warming bring? Science 317, 233–235.
Wilkie, K.M.K., Chapligin, B., Meyer, H., Burns, S., Petsch, S., Brigham-Grette, J., 2013. Modern isotope hydrology and controls on δD of plant leaf waxes at Lake El'gygytgyn, NE Russia. Clim. Past 9 (1).
Wilks, D.S., 1995. Statistical Methods in the Atmospheric Sciences. International Geophysics Series, vol. 59.
Wing, S.L., Harrington, G.J., Smith, F.A., Bloch, J.I., Boyer, D.M., Freeman, K.H., 2005. Transient floral change and rapid global warming at the Paleocene–Eocene boundary. Science 310, 993–996.
Wright, J.D., Schaller, M.F., 2013. Evidence for a rapid release of carbon at the Paleocene–Eocene thermal maximum. Proc. Natl. Acad. Sci. USA 110 (40), 15908–15913.
Xie, S., Nott, C.J., Avsejs, L.A., Volders, F., Maddy, D., Chambers, F.M., Gledhill, A., Carter, J.F., Evershed, R.P., 2000. Palaeoclimate records in compound-specific δD values of a lipid biomarker in ombrotrophic peat. Org. Geochem. 31, 1053–1057.
Yang, H., Liu, W.G., Leng, Q., Hren, M.T., Pagani, M., 2011. Variation in *n*-alkane delta D values from terrestrial plants at high latitude: implications for paleoclimate reconstruction. Org. Geochem. 42, 283–288.
Zachos, J.C., Wara, M.W., Bohaty, S., Delaney, M.L., Petrizzo, M.R., Brill, A., Bralower, T.J., Premoli-Silva, I., 2003. A transient rise in tropical sea surface temperature during the Paleocene–Eocene Thermal Maximum. Science 302, 1551–1554.
Zachos, J.C., Kroon, D., Blum, P., the Leg 208 Scientific Party, 2004. ODP Leg 208: the early Cenozoic extreme climates transect along Walvis Ridge. JOIDES J. 30, 8–13.
Zachos, J.C., Röhl, U., Schellenberg, S.A., Sluijs, A., Hodell, D.A., Kelly, D.C., Thomas, E., 2005. Rapid acidification of the ocean during the Paleocene–Eocene thermal maximum. Science 308, 1611–1615.
Zachos, J.C., Schouten, S., Bohaty, S., Quattlebaum, T., Sluijs, A., Brinkhuis, H., Gibbs, S.J., Bralower, T.J., 2006. Extreme warming of mid-latitude coastal ocean during the Paleocene–Eocene Thermal Maximum: inferences from TEX_{86} and isotope data. Geology 34, 737–740.
Zachos, J.C., Bohaty, S.M., John, C.M., McCarren, H., Kelly, D.C., Nielsen, T., 2007. The Paleocene–Eocene carbon isotope excursion: constraints from individual shell planktonic foraminifer records. Philos. Trans. R. Soc. 365, 1829–1842.